Charge segregation in weakly ionized microgels

John S. Hyatt, Alison M. Douglas, Chris Stanley, Changwoo Do, Thomas H. Barker, and Alberto Fernández-Nieves

Phys. Rev. E **95**, 012608 — Published 19 January 2017

DOI: 10.1103/PhysRevE.95.012608

Charge Segregation in Weakly-Ionized Microgels

John S. Hyatt,[1] Alison M. Douglas,[2] Chris Stanley,[3] Changwoo Do,[3] Thomas H. Barker,[4] and Alberto Fernández-Nieves[1]

[1] *School of Physics, Georgia Institute of Technology, Atlanta, GA 30332-0430, USA*
[2] *Wallace H. Coulter Department of Biomedical Engineering, Georgia Institute of Technology, Atlanta, GA 30332*
[3] *Biology and Soft Matter Division, Neutron Sciences Directorate, Oak Ridge National Laboratory, Oak Ridge, TN 37831, USA*
[4] *Department of Biomedical Engineering, University of Virginia, Charlottesville, VA 22908*

(Dated: December 14, 2016)

We investigate microgels synthesized from N-isopropylacrylamide (NIPAM) copolymerized with a large mol% of acrylic acid (AAc), finding that when the acid groups are partially ionized at high temperatures, competition between ion-induced swelling and hydrophobic deswelling of poly(NIPAM) chains results in microphase separation. In crosslinked microgels, this manifests as a dramatic decrease in the ratio between the radius of gyration and the hydrodynamic radius to ~ 0.2, indicating that almost all the mass of the microgel is concentrated near the particle center. We also observe a concurrent decrease of the polymer network length scale via small-angle neutron scattering, confirming the presence of a dense, deswollen core surrounded by a diffuse, charged periphery. We compare these results to those obtained for a system of charged ultra-low-crosslinked microgels (ULCs); the form factor shows a distinct peak at high q when the temperature exceeds a threshold value. We successfully fit the form factor to theory developed to describe scattering from weakly-charged gels in poor solvents and tie this behavior to charge segregation in the case of the crosslinked microgels.

I. INTRODUCTION

poly(N-isopropylacrylamide) (pNIPAM) microgels have been widely studied for their thermoresponsive properties in water. Depending on the solvent quality, which is a function of temperature, and the amount of crosslinker included in the synthesis, these particles can exhibit structural features spanning the colloid-to-polymer spectrum. Core-shell morphologies in particular can arise from reaction kinetics during synthesis that promote more crosslinker consumption during the initial stages [1, 2], leading to a more compact core surrounded by a fuzzy shell; in the extreme case of very high crosslinker concentration, or when high temperatures cause the pNIPAM and water to phase separate, the particles can approximate hard spheres [3, 4]. Other morphologies are available as well, such as grafting a shell of pNIPAM onto a compositionally different core [5] or copolymerizing NIPAM with another monomer, which can lead to different single-particle phase behavior. However, all of these cases share the broad similarity that the limiting behavior in the most-deswollen case is that of homogeneous spheres.

Using microgels composed of NIPAM copolymerized with acrylic acid (AAc) and crosslinked with poly(ethylene glycol) diacrylate (pEG-d), we recently showed that at pH 3, where the AAc is uncharged, this copolymer can frustrate the collapse of pNIPAM at high temperatures, leading to heterogeneous clumping of polymer within the particle and concentration of mass at the periphery [6]. In this work, we observe a segregation of mass at the particle center of the same particles due to a completely different mechanism when the AAc groups are partially charged. Specifically, we measure the radius of gyration, $R_{\rm g}$, defined as the root mean square distance of the mass elements of a particle from its center of mass, and the hydrodynamic radius, $R_{\rm h}$, which represents the overall particle size, and obtain the ratio $R_{\rm g}/R_{\rm h}$. Note that high and low $R_{\rm g}/R_{\rm h}$ values mean that the mass of a particle is concentrated far from or near to the center of mass, respectively. We obtain that $R_{\rm g}/R_{\rm h}$ decreases from ~ 0.5 to ~ 0.2 as T increases. The theoretical value for a sphere with homogeneous density is $R_{\rm g}/R_{\rm h} = \sqrt{3/5} \approx 0.775$. These results are consistent with static light scattering (SLS) measurements that show the particles conform to a core-shell model at low T and a star-polymer-like model at high T, and with small-angle neutron scattering (SANS) measurements that show the polymer network length scale decreases in tandem with $R_{\rm g}/R_{\rm h}$ as T increases. Equivalent measurements performed on ultra-low crosslinked (ULC) microgels [7], synthesized without added crosslinker, allow us to determine that these phenomena can be explained in terms of a theory developed for weakly-charged macrogels in a poor solvent [8].

II. CROSSLINKED MICROGELS

Our crosslinked microgels are comprised of 24 mol% AAc randomly copolymerized with NIPAM and crosslinked with 3 mol% pEG-d, $C_3H_3O(C_2H_4O)_nC_3H_3O_2$ (see Appendix A), where $n \approx 10$–11 is the number of repeat units. All measurements are made at pH 5, where the AAc is partially ionized, without any added salt. We perform SLS on dilute samples to obtain the form factor $P(q)$ directly from the measured intensity. At low T, we observe a

shallow minimum at intermediate values of the magnitude of the scattering wave vector, q. This minimum shifts to higher q as T increases and eventually disspears at sufficiently high temperature, as shown in Fig. 1a.

We fit the data with a form factor model incorporating polydispersity with a Gaussian distribution of width $\sigma_{\rm p}$,

$$P(q) = \frac{1}{\sqrt{2\pi}\sigma_{\rm p}\langle R\rangle}\frac{1}{\langle V^2\rangle}\int {\rm d}R\ V^2(R)\ P_1(q,R) \times \exp\left[-\frac{1}{2}\left(\frac{R-\langle R\rangle}{\sigma_{\rm p}\langle R\rangle}\right)^2\right] + I_1\frac{\Gamma(\mu)}{q\xi}\frac{\sin[\mu\arctan(q\xi)]}{[1+(q\xi)^2]^{\mu/2}} + I_0, \quad (1)$$

where the integral is over a distribution of monodisperse form factors $P_1(q,R)$ that dominate at low q and the squared particle volume divided by the mean squared volume, $V^2/\langle V^2\rangle$, which is included to account for the fact that the scattering length density of a particle is proportional to its volume squared. The second term models the scattering from the polymer network at small length scales, and I_0 is a constant accounting for the background scattering contribution. Depending on T and pH, $P_1(q,R)$ in Eq. 1 is one of the two monodisperse form factors:

$$P_1^{\rm CS}(q,R_{\rm c}) = \left[3\frac{\sin(qR_{\rm c})-qR_{\rm c}\cos(qR_{\rm c})}{(qR_{\rm c})^3}\right]^2\exp\left[-(q\sigma_{\rm s})^2\right] \quad (2a)$$

$$P_1^{\rm star}(q,R_{\rm g}) = \exp\left[-(qR_{\rm g})^2/3\right]. \quad (2b)$$

Eqs. 2a and 2b represent the core-shell [4] and star polymer [9] form factors. In the core-shell case, $R_{\rm c}$ and $2\sigma_{\rm s}$ are the core radius and approximate thickness of the fuzzy shell, respectively. We consider polydispersity in $R_{\rm c}$ only; considering polydispersity in only the shell results in worse results, and considering polydispersity in both the core and the shell does not improve the fit and adds an additional fitting parameter. The volume in Eq. 1 is $V=(4\pi/3)R_{\rm c}^3$, and the overall radius of the particle is given by $R_{\rm SLS}=R_{\rm c}+2\sigma_{\rm s}$. In the star polymer case, $R_{\rm g}$ is the radius of gyration and we take $V=(4\pi/3)R_{\rm g}^3$. The second term in Eq. 1 is a network term as derived originally in the context of star polymers [9], where Γ is the gamma function, $\mu=D_{\rm f}-1$, with $D_{\rm f}$ the polymer fractal dimension, and ξ represents a characteristic length scale. For $\mu=1$, this term reduces to a Lorentzian and ξ is the polymer correlation length. For $\mu=2$, the second term in Eq. 1 corresponds to a Debye-Bueche network term corresponding to a inhomogeneous scattering medium with a characteristic length scale ξ. For other values of μ, the physical interpretation of ξ is less obvious.

We see good agreement between our SLS data and Eq. 1, as shown in Fig. 1a. During the fit we vary $\langle R_{\rm c}\rangle$ and $\sigma_{\rm s}$, when fitting with Eq. 2a, or $\langle R_{\rm g}\rangle$, when fitting with Eq. 2b; these are shown in Table I. In both cases, we also leave $\sigma_{\rm p}$ as free parameter. We find that Eq. 2a applies at

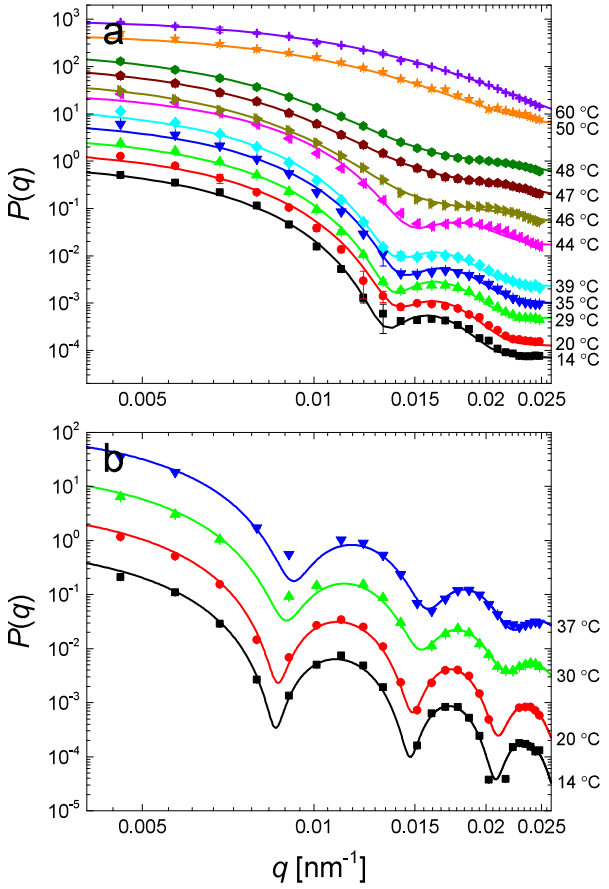

FIG. 1. P(q) obtained from SLS of dilute samples as a function of temperature (listed to the right of each graph) for (a) crosslinked microgels at pH 5, and (b) ULC microgels at pH 7.4. Lines represent fits to Eq. 2a for all measurements made with $T\leqslant 44$ °C, and Eq. 2b for all other measurements. The data have been vertically scaled for clarity.

$T\leq 44^o$C, while Eq. 2b applies at higher temperatures. We note that the radius of gyration can be obtained from all of our measured form factors. At low q, all form factors share the same dependence on $R_{\rm g}$, regardless of the detailed particle structure [10]: for $qR_{\rm g}\lesssim 2.5$, we obtain the usual Guinier decay, $P(q)\sim\exp[-(qR_{\rm g})^2/3]$. In the star polymer case, this function describes the entire q-range we probe; however, the Guinier decay appears at low q regardless of the exact form of $P(q)$. By fitting the low-q portion of our SLS data at $T\leq 44$ °C to this decay, we obtain the values of $R_{\rm g}$ shown in Table I. The values of σ_p are also shown in Table I.

The hydrodynamic radius of our particles, $R_{\rm h}$, is also shown in the table as a function of T. To obtain $R_{\rm h}$, we obtain the diffusion coefficient D of the particles from the electric field cross-correlation function measured via DLS, which has an exponential decay in Dq^2. We do this for many different q and fit to obtain D, which is related to $R_{\rm h}$ by the Stokes-Einstein relation, $R_{\rm h}=k_{\rm B}T/6\pi\eta_{\rm s}D$, where $k_{\rm B}$ is the Boltzmann constant and $\eta_{\rm s}$ the solvent viscosity. We find that across all temperatures for which

TABLE I. Values of the fitting parameters in Eq. 1 obtained from the data shown in Fig. 1. Where applicable, R_g obtained from the Guinier fit described in the text is shown as well.

T [°C]	R_h [nm]	$\langle R_c \rangle$ [nm]	$2\sigma_s$ [nm]	R_{SLS} [nm]	R_g [nm]	σ_p
(crosslinked microgels)						
14	680 ± 30	341 ± 10	198 ± 20	539 ± 30	324 ± 14	0.065 ± 0.015
20	670 ± 30	325 ± 10	191 ± 10	516 ± 20	330 ± 25	0.073 ± 0.008
29	670 ± 40	331 ± 4	186 ± 10	517 ± 14	333 ± 8	0.06 ± 0.01
35	570 ± 30	322 ± 6	182 ± 10	504 ± 16	343 ± 8	0.07 ± 0.01
39	710 ± 30	339 ± 10	191 ± 18	530 ± 28	347 ± 12	0.074 ± 0.01
44	710 ± 30	312 ± 5	144 ± 10	456 ± 15	329 ± 4	0.09 ± 0.01
46	820 ± 40				319 ± 14	0.07 ± 0.06
47	830 ± 30				298 ± 13	0.08 ± 0.07
48	730 ± 30				298 ± 13	0.13 ± 0.06
50	630 ± 80				222 ± 21	0.23 ± 0.05
60	760 ± 30				183 ± 9	0.23 ± 0.01
(ULC microgels)						
14	626 ± 22	527 ± 5	36 ± 30	563 ± 35	460 ± 5	0.03 ± 0.01
20	593 ± 17	523 ± 5	37 ± 30	560 ± 35	455 ± 10	0.03 ± 0.01
30	567 ± 14	511 ± 5	23 ± 20	534 ± 25	440 ± 10	0.06 ± 0.02
37	592 ± 24	495 ± 5	44 ± 40	539 ± 45	420 ± 10	0.05 ± 0.02

we were able to apply the core-shell model, R_h is $\sim 20\%$ larger than R_{SLS}, likely due to lower polymer density at the particle periphery. This periphery contributes more strongly to drag, leading to a higher value of R_h, than to the scattered intensity, leading to a lower value of R_{SLS}.

We find that while R_g decreases with increasing T for our crosslinked microgels, R_h, the hydrodynamic radius measured by DLS, remains roughly constant (see Fig. 2a). The ratio R_g/R_h is a measure of the scattering length density inside the particle. However, given that the refractive indices of our monomers are similar (~ 1.52 for NIPAM [11, 12] and ~ 1.42 for AAc [13]), they scatter light approximately the same and the ratio can thus be interpreted as a measure of the mass distribution inside the particle. Hence, R_g/R_h can be taken to correspond to the ratio of the root-mean-square distance of the particle components from the center of mass to the overall size of the particle. For homogeneous spheres, $R_g/R_h = \sqrt{3/5}$. At low temperatures, we find $R_g/R_h \sim 0.5$ for our crosslinked microgels, consistent with the core-shell model, which assumes a higher density at the particle center. Similar results have also been observed in branched macromolecules [14, 15]. Remarkably, at high temperatures, this ratio decreases to ~ 0.2, as shown in Fig. 2b. To our knowledge, the lowest R_g/R_h previously measured for microgels is ~ 0.5. This indicates an unusually dense, small core. For crosslinked pNIPAM microgels synthesized without AAc or another comonomer, R_g/R_h typically increases with T, approaching the homogeneous sphere value at high T [4]. Previous experiments performed on the same crosslinked microgels used in this study found R_g/R_h to increase above $\sqrt{3/5}$ at high T and low pH, where the AAc groups are not ionized [6]. Thus, since the only difference in the pH 5 suspensions of crosslinked microgels in this study is the presence of partially ionized AAc, the decreasing and unusually low R_g/R_h must be a direct consequence of charge.

Borue and Erukhimovich (BE) developed a statistical mechanics theory for partially ionized polyelectrolytes in solvents of varying quality [8]. This theory has successfully described the behavior of weakly charged macrogels in a bad solvent [16]. In these systems, the polymer component that favors demixing from the solvent at high T tends to contract the gel network, which has the secondary effect of localizing the charged groups of the network into a smaller volume. To maintain electroneutrality, the counterions in the solvent must follow these charges, and are therefore likewise confined; this imposes an entropic cost on the counterions. The system can offset this cost by allowing the polymer network to locally swell near the charged groups, increasing the volume available to the localized counterions and resulting in a spatial fluctuation in polymer concentration depending on the distribution of charges.

Two parameters in BE theory govern the phase behavior of the system. The first is the reduced charge concentration, written in dimensionless form as

$$s = (\kappa r_0)^2, \tag{3}$$

where $\kappa^{-1} = \sqrt{(R_h)^3/(3\ell_B Q)}$ is the Debye length for a spherically symmetric microgel particle, with ℓ_B the Bjerrum length and Q the number of charges in the microgel, and r_0 is the screening length that would exist solely due to charges in the polymer if it were in an ion-free solution. This length scale is given by

$$\begin{aligned} r_0 =& a\left(\frac{48\pi\ell_B}{a}\phi_p\alpha^2\right)^{-1/4} \\ &\times \begin{cases} \left[1+\left(\frac{1-2\chi}{2\phi_p}\right)^{1/2}\right]^{1/8} & \chi < \frac{1}{2} \\ 1 & \chi \geqslant \frac{1}{2} \end{cases}, \end{aligned} \tag{4}$$

where $a \approx 0.25$ nm is the length of a monomer, ϕ_p is the

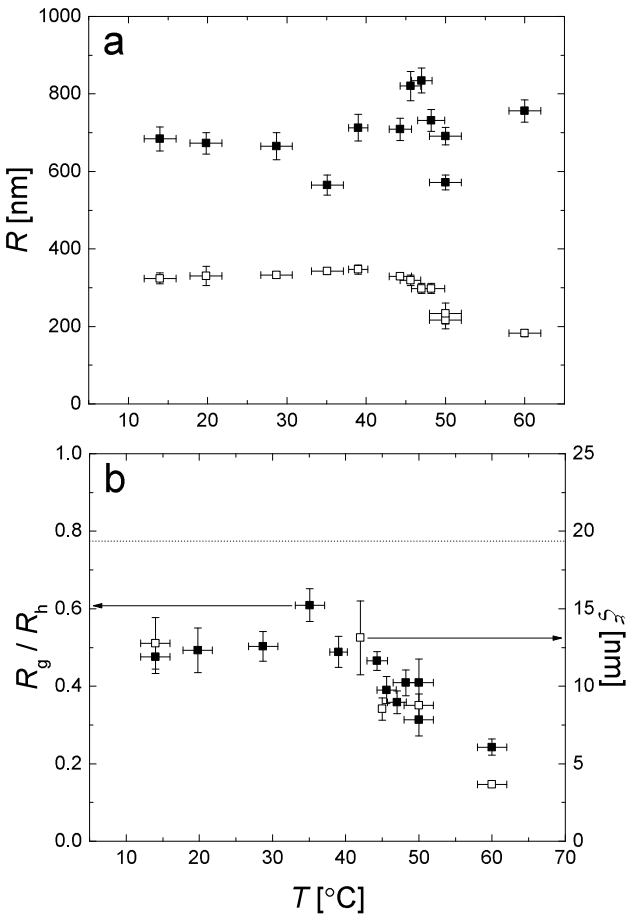

FIG. 2. Light scattering and SANS length scales for crosslinked microgels at pH 5 as functions of temperature. (a) $R_{\rm h}$ (filled symbols) and $R_{\rm g}$ (open symbols). (b) $R_{\rm g}/R_{\rm h}$ (closed symbols, left axis) and ξ (open symbols, right axis), showing the corresponding decrease in the two quantities as T increases. The dashed black line shows the value of $R_{\rm g}/R_{\rm h}$ for homogeneous spheres.

volume fraction occupied by monomer inside a microgel, α is the degree of ionization of the monomers, and χ is the temperature-dependent Flory solvency parameter. For the Flory parameter of pNIPAM in heavy water, which is the solvent used in our SANS measurements, we use [17]

$$\chi = \frac{1}{2} + 25\left(1 - \frac{306.5\ \mathrm{K}}{T}\right). \tag{5}$$

The second governing parameter in BE theory is the reduced temperature, written in dimensionless form as

$$t = -12\left(\frac{r_0}{a}\right)^2\left[\frac{-a^3(1-2\chi) - 3B_3\phi_{\rm p}}{a^3}\right]\phi_{\rm p}, \tag{6}$$

where B_3 is the third virial coefficient.

For our crosslinked microgels, we estimate $Q = (6 \pm 5) \times 10^7$ and $\alpha = 0.195$, and a value $\phi_{\rm p} = 0.011 \pm 0.004$, averaged over the entire particle, at $T = 60$ °C (see Appendix B). This results in $r_0 = 0.40 \pm 0.04$ nm, $\kappa^{-1} = 1.2 \pm 0.2$ nm and $s = 0.11 \pm 0.01$ at $T = 60$ °C. Estimating t is not possible without knowing B_3. However, for a poor solvent, $t < 0$. In our case, we observe a decreasing $R_{\rm g}$ with increasing T for $T \gtrsim 40$ °C, indicating the solvent quality decreases as T increases. Furthermore, since T is larger than the lower critical solution temperature of pNIPAM, at these high T, we are confident the solvent quality is poor.

The behavior of a polymer system on the edge of demixing is determined by the Helmholtz free energy. For a two-phase system such as ours, the binodal, which defines the conditions where phase coexistence is favorable, is defined by the set of points where both components have equal chemical potentials in both phases. The set of points where the second derivative of the Helmholtz free energy is zero defines the spinodal. The binodal and spinodal coincide at the critical point, where the phases can no longer be distinguished. The overall behavior is thus reminiscent of that of a van der Waals fluid. Outside the binodal, the thermodynamically stable state is a single-phase state. In the region between the binodal and the spinodal, the system is metastable and can only phase separate in the presence of large enough fluctuations. In contrast, in the region enclosed by the spinodal, the system is unstable to arbitrarily small fluctuations.

Interestingly, unlike a van der Waals fluid, polyelectrolyte systems can either macrophase or microphase separate. The first situation corresponds to the familiar phase coexistence of polymer-rich and polymer poor phases. In contrast, microphase separation results when this coexistence occurs locally and not at macroscopic scales; this ultimately reflects the existence of an underlying cause or constraint that prevents the system from macrophase separating. In BE theory, this situation is expected for $t < 1$ and $s < 1$. In this case, the solvent quality is poor and there is a desire for the system to reduce its overall volume. However, the entropic penalty associated with decreasing the overall volume accessible to the counterions opposes macrophase separation and results in the formation of polymer-rich and polymer poor microdomains. This happens without a significant overall volume change, leaving nearly the same amount of accessible volume to the counterions. Specifically, microphase separation is expected in BE theory if the system is below the spinodal curve, which is defined by $s - t = 2$. We believe that the low values of R_g/R_h we observe experimentally originate from the proximity of our system to the spinodal line. We note, however, that while BE theory applies to homogenous systems, our microgels have more crosslinker at their core than at their periphery.

To test our interpretation, we recall that BE theory predicts a measurable signature in the form factor for a system in this region, namely a peak in $P(q)$ at large q whose form is given by

$$P(q) = \frac{I_2}{x^2 + t + 1/(x^2 + s)}, \tag{7}$$

where $x = qr_0$ and I_2 determines the peak height. This function is peaked at $q_{\rm peak} = \sqrt{r_0^{-2} - \kappa^2}$, which corresponds to a characteristic length scale, $2\pi/q_{\rm peak}$, associated to the correlations due to the presence of concentration fluctuations or microphase separation. We then perform SANS experiments to extend the q range accesible with light to higher values. All SANS measurements were conducted on the EQ-SANS instrument at the Spallation Neutron Source at Oak Ridge National Laboratory using sample-to-detector distances of 4 and 2.5 m, and minimum wavelengths of 9.5 and 2.5 Å, respectively. The measured scattering intensity was corrected for detector sensitivity, instrument resolution and the background from the empty cell and the solvent, and was radially averaged over the detector [18].

The experimental results are shown in Fig. 3a. Note that the BE theory peak is not present in our data; our estimates predict that $q_{\rm peak} \approx 2.5$ nm^{-1}, which is outside the available range of the instrument, and well into the region in which the background dominates the scattering. Instead, we fit the data to the second term in Eq. 1, which dominates in this range of q. The resulting values of ξ are plotted against the right-hand axis in Fig. 2; remarkably, they show a decrease with T that closely tracks the $R_{\rm g}/R_{\rm h}$ obtained from light scattering. Further, at $T = 60$ °C, $\xi = 3.7 \pm 0.1$ nm, which agrees well with the $2\pi/q_{\rm peak} \approx 2.5$ nm predicted by BE theory.

III. ULTRA-LOW CROSSLINKED MICROGELS

To further test our interpretation of our results in terms of BE theory, we perform similar sets of measurements on microgels synthesized without added crosslinker. These microgels are synthesized with 5 mol% AAc (see Appendix A); because the AAc content of the polymer is lower than in our crosslinked microgels, a higher fraction of the AAc must be ionized to obtain a similar charge fraction. We therefore perform measurements on the ULCs at pH 7.4 to ensure we are in a regime of similar s. This combination of synthesis and measurement parameters is expected to result in a BE theory peak in the q range accessible with SANS. Furthermore, these microgels closely approach monodisperse, homogeneous spheres; SLS measurements of dilute samples are well described by Eqs. 1 and 2a, as shown in Fig. 1b, and result in R_g/R_h values that are always close to $\sqrt{3/5}$. The resulting fitting parameters are included in Table I.

The SANS data exhibit the distinctive peak predicted by BE theory for $T \geqslant 43$ °C. In addition, Eq. 7 succesfully describes the experimental observations, as shown in Fig. 3b. The lines in this figure are fits to the data with s and t as fitting parameters; these lie just below the line $s - t = 2$, for suffciently high T, as shown in Fig. 4. The ULC system is thus just inside the microphase-separated region at high T.

The ULC results corroborate our interpretation of the

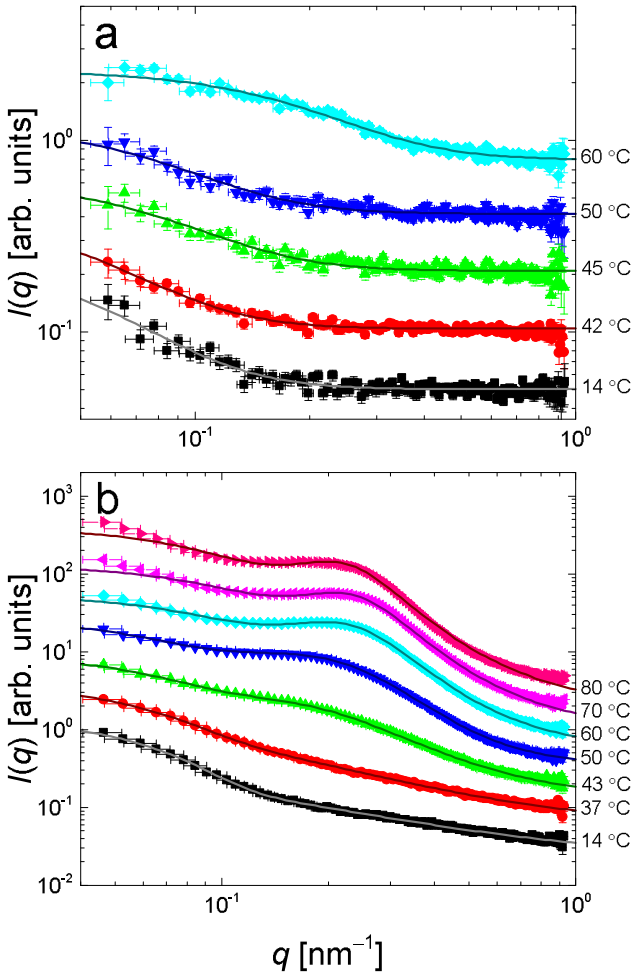

FIG. 3. SANS scattering profiles measured for (a) crosslinked microgels at pH 5 and (b) ULC microgels at pH 7.4. Lines are fits to Eq. 1 for the crosslinked microgels and for the $T = 14$ °C and 37 °C ULCs and Eq. 7 otherwise. Note the distinctive scattering peak in the ULC microgels in (b) at high T. Note that the initial decay and the high-q background in the fits to Eq. 7 are both remainders from Eq. 1. The data have been vertically scaled for clarity.

data for the crosslinked microgels. As T increases above about 40 °C, the measured values of ξ and $R_{\rm g}/R_{\rm h}$ both decrease. At the same time, $P(q)$ gradually undergoes a qualitative shape change, with the model best describing the data transitioning from core-shell at low T to star-polymer-like at high T. At intermediate T, between 40–45 °C, the measured $P(q)$ has traits of both models. As T increases, the core is contracting and densifying, while the periphery is expanding and becoming more diffuse, leading to a conformation reminiscent of a star polymer with a dense core. The driving force for this change is the proximity of the microgel to the microphase separation predicted by BE theory; the core, having a higher crosslink density and therefore a higher $\phi_{\rm p}$, has a lower s and t than the periphery. Thus the solvent quality is effectively higher in the periphery than at the core, lead-

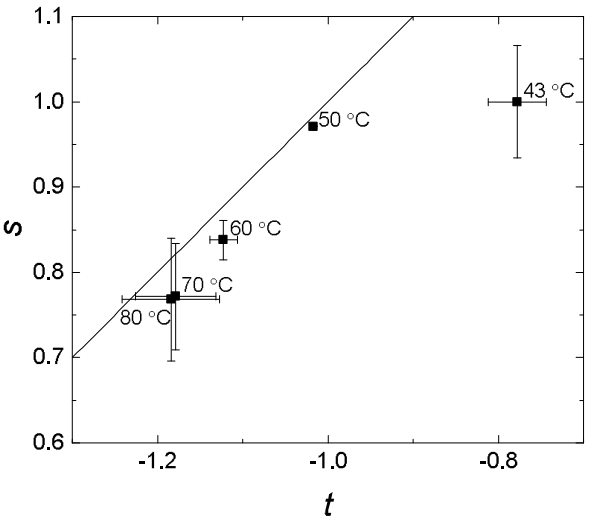

FIG. 4. Values of s and t obtained from fits of Eq. 7 to the SANS scattering profiles shown in Fig. 3b at high T. The black line is the spinodal, $s - t = 2$.

ing to a more swollen state in the periphery. Finally, the denser core scatters neutrons more strongly than the diffuse periphery, and therefore contributes disproportionally to the intensity measured with SANS. This explains why only the decreasing ξ of the core, and not the (presumably increasing) ξ of the periphery, is observed in our SANS measurements.

We emphasize that the observed morphological changes happen without significant changes in $R_{\rm h}$, which is a hallmark of microphase separation. In this case, the large swollen periphery and the small dense particle core enable the average counterion distance to be effectively maintained inside the microgel. It is the contribution of the counterions to the system free energy, which disfavors macrophase separation, and the inhomomegous crosslinker distribution inside the particles, that seems to combine to result in the observed paricle morphology.

IV. CONCLUSIONS

Our results confirm the applicability of BE theory to microgels. For ULCs, which have a very homogeneous distribution of polymer, the theory can be applied directly to fit the measured form factor at high q. For crosslinked microgels, the original assumptions of the theory, particularly, that the polymer distribution is homogeneous throughout the network, must be carefully considered; nevertheless, the theory itself is still useful if the details of the microgel structure are taken into account. We note that these structural details need to always be considered with care, particularly when comparing microgels synthesized via different means; this applies to both the crosslinker and AAc distribution, which can also be inhomogeneous [19]. Overall, our results suggest another mechanism by which the comonomer can influence the internal structure of a microgel particle, and present a path for generating microgels with very low $R_{\rm g}/R_{\rm h}$ values.

V. ACKNOWLEDGEMENTS

We thank financial support from the National Science Foundation (DMR-1609841), and X. Hu and L. A. Lyon for the syntehsis of the crosslinked microgels. Research conducted at ORNL's Spallation Neutron Source was sponsored by the Scientific User Facilities Division, Office of Basic Energy Sciences, US Department of Energy. We also thank the research partnership between Childrens Healthcare of Atlanta and the Georgia Institute of Technology, and Michael Dimitriev for useful discussions.

Appendix A: Microgel synthesis

1. Crosslinked microgels

We follow a dispersion polymerization synthesis according to previously published methods [20]. We add 9.08 g (73 mol%) of NIPAM, 1.92 g (3 mol%) of pEGd (molecular weight 587 g/mol), 1.9 g (24 mol%) of AAc, 0.058 g of sodium dodecyl sulfate (a surfactant), and 0.342 g of ammonium persulfate (the reaction initator) to 1587 mL of dionized water at 70 ^{o}C. We allow the reaction to proceed for 8 hours while stirring at 350 rpm, then cool the dispersion to room temperature and remove aggregates by filtering through glass wool. To remove unreacted monomer, cross-linker, surfactant, and initiator molecules, we dialyze the suspension against dionized water refreshed daily for four weeks using a Spectra/Por dialysis membrane. The membrane was previously sterilized by boiling and has a molecular weight cutoff of 12,000-14,000 g/mol.

2. Ultra-low crosslinked microgels

Ultra-low crosslinked microgels of poly(N-isopropylacrylamide-co-acrylic acid) were synthesized from standard precipitation polymerization techniques as previously described in [7, 21–23]. Sterile filtered solutions of NIPAM monomer (1.5g, recrystallized from n-hexanes; this corresponds to 95 mol % of the particle monomer) dissolved in dionized water were added to a 3-neck round bottom reaction vessel immersed in an oil bath at 70 ^{o}C and mixed at 450 rpm while purging with N_2 until the temperature was stable. Acrylic acid (0.05g, corresponding to 5 mol % of the particle monomer), was added after the solution reached the desired temperature and 10 minutes before the addition of the reaction initiator, ammonium persulfate (0.0228g - 1mM) for a final reaction volume of 100 ml. The reaction then proceeded

for 6 hours, after which the solution of microgels was cooled and filtered through glass wool. The microgels were purified by ultra-centrifugation through pelleting and redispersing in dionized water 5 times. Purified microgels were then lyophilized for future use.

Appendix B: Estimating the Fraction of Charged Groups in Crosslinked Microgels

To determine the s and t values of our crosslinked microgels, we need a way to estimate the values of the parameters Q, α, and $\phi_{\rm p}$. We perform estimates of Q and α via two independent methods, both of which allow us to obtain the relationship between mass and volume for the particles in the desired states. In the first, we experimentally obtain this relationship from viscometry measurements of dilute microgel suspensions. In the second, we use literature values of the bound fraction of water and polymer density in collapsed microgels. The results from both methods are consistent with one another.

1. Via Viscometry

The behavior of colloidal particles in suspension depends on whether and how the particles are interacting. For the simplest case of idealized hard spheres, the only interaction is excluded volume. The relevant thermodynamic quantity in this case is the volume fraction,

$$\phi = N v^{\rm P}/V, \tag{B1}$$

where N is the number of particles in the sample, $v^{\rm P} = (4\pi/3)R^3$ is the volume of one particle with radius R, and V is the total volume of the sample. ϕ can be related to concentration or weight fraction via the dynamic viscosity of the suspension, η, for dilute conditions using the Einstein-Batchelor equation [24–27]:

$$\eta/\eta_s = 1 + 2.5\phi + 5.9\phi^2, \tag{B2}$$

where η_s is the viscosity of the solvent. The volume fraction is given by $\phi = kc$, where c is a measure of the suspension concentration and k is a constant. In our analysis we use weight percent, $c = [m_{\rm dry}/(m_{\rm dry} + m_{\rm solvent})] \times 100\%$. From Eq. B2 and a plot of $\eta/\eta_{\rm s}$ vs. c, we obtain k, shown in Fig. 6.

Suppose we have a suspension of some c, at conditions for which we have already measured k. By changing T and/or pH, we change k and therefore ϕ, even though c is fixed. However, because $\phi \propto R^3$, we can determine the new k if we know R in both conditions. Taking $R = R_{\rm h}$, we obtain k from the following relationship:

$$\frac{k(T_1, {\rm pH}_1)}{k(T_2, {\rm pH}_2)} = \left[\frac{R_{\rm h}(T_1, {\rm pH}_1)}{R_{\rm h}(T_2, {\rm pH}_2)}\right]^3. \tag{B3}$$

In addition to the measurements shown in Fig. 2a, we have measured the hydrodynamic radius of our crosslinked microgels for a wide variety of conditions, as shown in Fig. 5.

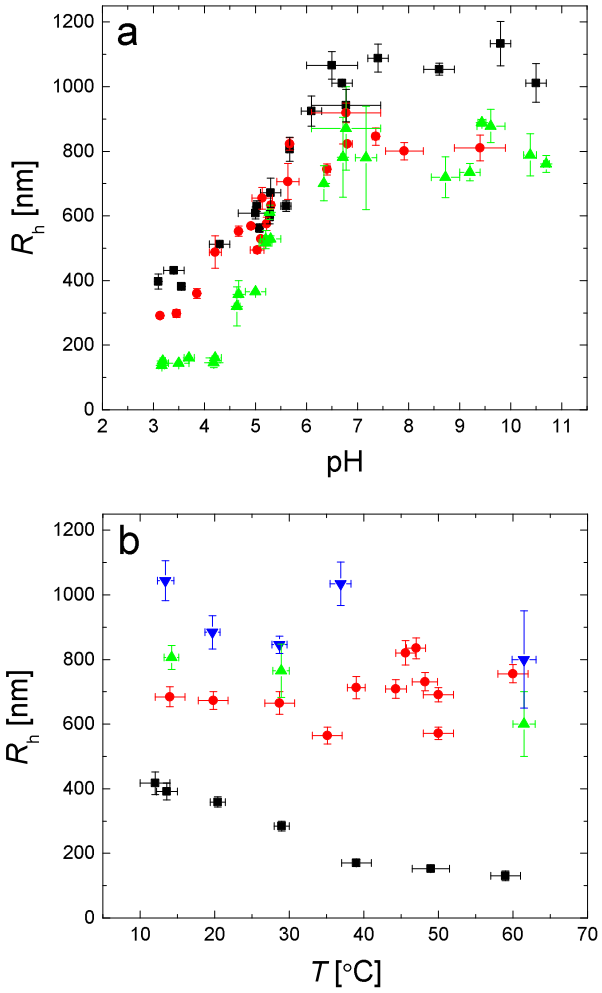

FIG. 5. (a) $R_{\rm h}$ as a function of pH for $T = 14 \pm 1$ °C (black squares), $T = 29 \pm 1$ °C (red circles), and $T = 58 \pm 3$ °C (green triangles). (b) $R_{\rm h}$ as a function of T for pH = 3.1 (black squares), pH = 5.0 (red circles), pH = 5.7 (green upward triangles), and pH = 6.5 (blue downward triangles).

We perform viscometry measurements on suspensions over a range of concentrations at pH $= 3.99 \pm 0.07$ and 4.54 ± 0.19, and $T = 14.1$, 24.4, 30.1, 38.9, and 58.3 °C ($\delta T \leqslant 0.1$ °C for all measurements). We use an Ubbelohde viscometer manufactured by Technical Glass Products, Inc., with a viscometer constant of 0.003121 cSt/s at all temperatures. We ensure uniform temperature throughout the measurement by immersing the viscometer in a heated or cooled water bath whose temperature we measure via thermocouple during the experiment and allowing the temperature of the sample to equilibrate for at least 15 minutes prior to each measurement.

We measure six efflux times for each combination of T and pH, averaging them together to obtain the final value and uncertainty. By multiplying the efflux time by the viscometer constant, we obtain the kinematic viscosity, ν,

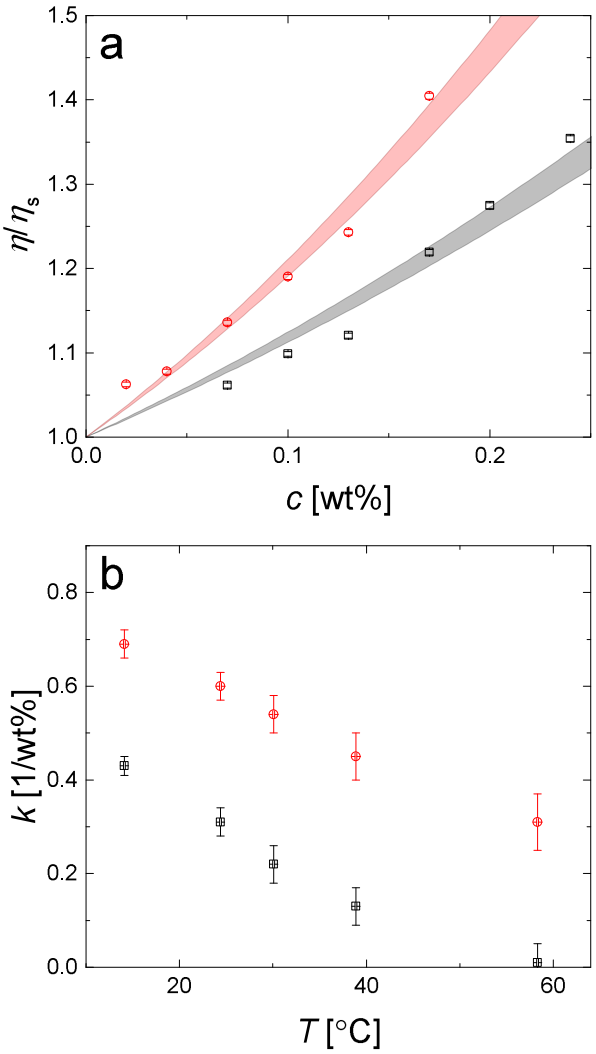

FIG. 6. Viscometry measurements for our crosslinked microgels at selected conditions. (a) Relative viscosity as a function of concentration for pH $= 3.99 \pm 0.07$ (black squares) and pH $= 4.54 \pm 0.19$ (red circles). For clarity, only one set of temperature measurements is shown, at $T = 14.1 \pm 0.1$ °C. Fits are to Eq. B2, with the width of the curve indicating uncertainty in k. (b) k values obtained from fitting the data to Eq. B2 as a function of temperature.

of the suspension, which is related to the dynamic viscosity, η, by $\nu = \eta/\rho$, with ρ the suspension density, which we take to be equal to that of water at the measured temperature. We obtain ρ for water as a function of temperature by interpolating the literature values [28]. After obtaining the dynamic viscosity of each suspension, we finally calculate the relative viscosity using the empirical Watson-Basu-Sengers equation [29] for the temperature-dependent viscosity of water. We fit the results with Eq. B2, as shown in Fig. 6.

To confirm that we can accurately calculate ζ for other conditions using Eq. B3, we compare k values from Fig. 6 with those calculated using Eq. B3 and find good agreement using values of $R_\mathrm{h}(T, \mathrm{pH})$ from Fig. 5. For example, the values of k at $T \sim 14$ °C are 0.43 ± 0.02 and 0.69 ± 0.03 for pH ~ 4 and ~ 4.5, respectively, giving $k(T = 14, \mathrm{pH} = 4)/k(T = 14, \mathrm{pH} = 4.5) = 0.6 \pm 0.1$. From Fig. 5 we find that at these conditions, $R_\mathrm{h} \approx 460 \pm 20$ nm and 550 ± 20 nm, respectively. From Eq. B3, we obtain the same ratio, $k = 0.6 \pm 0.15$. Following the same procedure, for the same pHs at $T = 28.7$ °C, we find the ratios of both k and R_h^3 to be 0.4 ± 0.1. Other conditions display a similar match. We therefore use Eq. B3 to calculate ζ for other values of T and pH. The error using this method is $\lesssim 10\%$, comparable to the error in the viscometry measurements themselves.

Using these values of k and R_h, we estimate the number of AAc monomers in our microgels. We consider a single microgel in Eq. B1 by setting $V = v^\mathrm{P}$ and $N = 1$, giving $1/k = c$. Rearranging the concentration to solve for the mass of polymer in a single microgel gives $m_\mathrm{p} = m_\mathrm{solvent}/(100\% \times k - 1)$. Approximating the density of the microgel as that of the solvent, in our case water, gives that the polymer mass per volume of the swollen particle follows $m_\mathrm{p} = \rho_\mathrm{water} v^\mathrm{P}/(100\% \times k - 1)$. This is equivalent to $m_\mathrm{p} = (4.2 \times 10^{-21}\ \mathrm{nm}^{-3}) R_\mathrm{h}^3/(100\% \times k - 1)$, with k in inverse wt%.

The total mass of a particle is given by the combined mass of its constituents. In terms of the three monomers included in the synthesis, this is $m_\mathrm{p} = n_\mathrm{NIPAM} m_\mathrm{NIPAM} + n_\mathrm{AAc} m_\mathrm{AAc} + n_\mathrm{pEG\text{-}d} m_\mathrm{pEG\text{-}d}$, where n_i is the number of moles and m_i the molar mass of component i. The synthesis includes 73 mol% NIPAM, 24 mol% AAc, and 3 mol% pEG-d, and the molar masses of these monomers are 113 g/mol, 72 g/mol, and 587 g/mol, respectively. Combining both expressions for m_p allows us to estimate n_AAc, shown in Table II.

TABLE II. Values for the number of moles of AAc, n_AAc, or equivalently the number of AAc monomers, N_AAc, estimated using parameters measured at several different conditions. $T = 14$ °C in all cases.

pH	R_h [nm]	k [wt%]	n_AAc [moles]	N_AAc
4	460 ± 20	0.43 ± 0.02	1.99×10^{-17}	1.20×10^7
4.5	550 ± 20	0.69 ± 0.03	2.10×10^{-17}	1.20×10^7
6.5	1040 ± 60	4.2 ± 0.2	2.05×10^{-17}	1.23×10^7

Averaging these three values, we obtain $n_\mathrm{AAc} = (2.05 \pm 0.06) \times 10^{-17}$ moles and equivalently $N_\mathrm{AAc} = (1.23 \pm 0.03) \times 10^7$.

2. Via Calculation from Literature Values

We estimate the number of monomers in one microgel. The amount of bound water in a deswollen pNIPAM microgel is about 0.39 ± 0.01 g of water per 1 g of polymer [30]. From Fig. 5, we estimate that $R_\mathrm{h} = 145 \pm 10$ nm for pH 3 and $T = 60$ °C, when the AAc is uncharged and the particle should be approximately as deswollen as a pNIPAM microgel. Given that the density of dry

pNIPAM is 1.1 g/cm^3 [31], and using this as the approximate density of dry pAAc and pEG-d, we can estimate the radius of a dry (completely deswollen, often referred to as "collapsed") microgel as $R_{\rm dry} = 129 \pm 9$ nm. We divide the volume of the dry microgel by the approximate volume of one monomer, $v_{\rm monomer} \approx 0.016$ nm^3, estimated by cubing the linear dimension of one monomer in a chain, ~ 0.25 nm. (Because NIPAM, AAc, and pEG-d all contribute two carbon-carbon bonds to the backbone of the polymer chain, the volume contributed by each one should be similar.) This gives approximately $(5.7 \pm 1.2) \times 10^8$ monomers in one microgel. 24% of these, or $(1.4 \pm 0.3) \times 10^8$, are AAc monomers.

3. Obtaining Q, α, and $\phi_{\rm p}$

Both methods give values that are comparable, given that the comparison is based on values obtained by two independent means, each with a corresponding error. We take the number of AAc to be the average of these two values, giving $N_{\rm AAc} = (8 \pm 6) \times 10^7$. The p$K_{\rm a}$ of AAc is 4.4. At pH 5, therefore, about 80% of AAc groups are charged: this translates to $Q = (6 \pm 5) \times 10^7$. Including all three monomer species, this gives $\alpha \approx 0.195$. Finally, we can estimate $\phi_{\rm p} = (R_{\rm dry}/R_{\rm h})^3 \approx 0.011 \pm 0.004$ at $T = 60$ °C.

[1] X. Wu, R. Pelton, A. Hamielec, D. Woods, and W. McPhee, Colloid Polym. Sci. **272**, 467 (1994).
[2] M. Seeber, B. Zdyrko, R. Burtovvy, T. Andrukh, C.-C. Tsai, J. Owens, K. Kornev, and I. Luzinov, Soft Matter **7**, 9962 (2011).
[3] I. Varga, T. Gilányi, R. Mészáros, G. Filipcsei, and M. Zrínyi, J. Phys. Chem. B **105**, 9071 (2001).
[4] M. Stieger, W. Richtering, J. Pedersen, and P. Lindner, J. Chem. Phys. **120**, 6197 (2004).
[5] T. Hellweg, J. Polym. Sci. Part B Polym. Phys. **51**, 1073 (2013).
[6] J. Hyatt, C. Do, X. Hu, H. Choi, J. Kim, L. Lyon, and A. Fernández-Nieves, Phys. Rev. E **92**, 030302(R) (2015).
[7] A. Brown, S. Stabenfeldt, B. Ahn, R. Hannan, K. Dhada, E. Herman, V. Stefanelli, N. Guzzetta, A. Alexeev, W. Lam, L. Lyon, and T. Barker, Nature Materials **13**, 1108 (2014).
[8] V. Borue and I. Erukhimovich, Macromolecules **21**, 3240 (1988).
[9] W. Dozier, J. Huang, and L. Fetters, Macromolecules **24**, 2810 (1991).
[10] J. Dhont, *An Introduction to Dynamics of Colloids*, 2nd ed. (Elsevier Science B.V., Amsterdam, 2003).
[11] M. Reufer, P. Díaz-Leyva, I. Lynch, and F. Scheffold, Eur. Phys. J. E **28**, 165 (2009).
[12] R. Chen, H. Yang, X. Yan, Z. Wang, and L. Li, Chem. J. Chin. U. **22**, 1262 (2001).
[13] *Acrylic Acid*, Base Acrylic Monomer Manufacturers, Inc. (2013), 4th Ed.
[14] W. Burchard, Adv. Polym Sci. **143**, 113 (1999).
[15] W. Burchard, Adv. Polym Sci. **48**, 1 (1983).
[16] M. Shibayama, T. Tanaka, and C. Han, J. Chem. Phys. **97**, 6842 (1992).
[17] M. Shibayama, T. Tanaka, and C. Han, J. Chem. Phys. **97**, 6829 (1992).
[18] J. Zhao, C. Gao, and D. Liu, J. Appl. Cryst. **43**, 1068 (2010).
[19] T. Hoare and M. D., J. Phys. Chem. B **110**, 20327 (2006).
[20] Z. Meng, M. Smith, and L. A. Lyon, Colloid Polym. Sci. **284**, 277 (2009).
[21] J. Gao and B. J., Langmuir **19**, 5212 (2003).
[22] J. Gao and B. J., Langmuir **19**, 5217 (2003).
[23] H. Bachman, A. Brown, K. Clarke, K. Dhada, A. Douglas, C. Hansen, E. Herman, J. Hyatt, P. Kodlekere, Z. Meng, S. Saxena, M. Spears Jr, N. Welsch, and L. Lyon, Soft Matter **11**, 2018 (2015).
[24] A. Einstein, Annln. Phys. **19**, 289 (1906).
[25] A. Einstein, Annln. Phys. **34**, 591 (1911).
[26] G. Batchelor, J. Fluid Mech. **83**, 97 (1977).
[27] J. Brady and M. Vicic, J. Rheol. **39**, 545 (1995).
[28] D. Lide, ed., *CRC Handbook of Chemistry and Physics*, 70th ed. (CRC Press, Boca Raton, Florida, 1990).
[29] J. Watson, R. Basu, and J. Sengers, J. Phys. Chem. Ref. Data **9**, 1255 (1980).
[30] A. Lele, M. Hirve, M. Badiger, and R. Mashelkar, Macromolecules **30**, 157 (1997).
[31] H. Schild, Prog. Polym. Sci. **17**, 163 (1992).